Zirconium oxide supported on Pd(100): characterization by scanning tunneling microscopy and tunneling spectroscopy

K. Asakura [1], Y. Iwasawa [1], S.K. Purnell [2], B.A. Watson [2], M.A. Barteau [2] and B.C. Gates [2]

[1] *Department of Chemistry, Faculty of Science, University of Tokyo, Bunkyo-ku, Tokyo 113, Japan*
[2] *Center for Catalytic Science and Technology, Department of Chemical Engineering, University of Delaware, Newark, DE 19716, USA*

Received 25 February 1992; accepted 10 June 1992

Scanning tunneling microscopy (STM) and tunneling spectroscopy (TS) were used to characterize the structure of a model metal-supported dispersed metal oxide, ZrO_2 on Pd(100). STM images illustrate changes in the surface morphology of the ZrO_2 resulting from various chemical treatments. When the sample was treated in O_2, the ZrO_2 appeared as a smooth, featureless overlayer of varying thickness wetting the Pd. After treatment in H_2, the ZrO_2 formed non-wetting particles on the Pd, with a sharp Pd–ZrO_2 interface. TS provided a fingerprint that verified the presence of a semiconducting overlayer on a metallic support. These results appear to be consistent with X-ray absorption spectra of ZrO_2 supported on Pd black, reported elsewhere.

Keywords: Zirconium oxide; palladium; scanning tunneling microscopy; tunneling spectroscopy

1. Introduction

Many practical catalysts consist of metal clusters or particles dispersed on metal oxide supports. The interactions between the metal and the underlying support affect catalyst structure and properties; however, notwithstanding extensive research with supported metals [1–3], understanding of the nature of the metal–support interface and its influence on catalyst performance is far from complete. ZrO_2 is of interest as a support [4–6] because there is evidence of significant support effects leading to modification of the catalytic properties of metal particles [7,8]. Two-dimensional films of Rh and Pt form on ZrO_2 at low temperature, and exposure to O_2 leads to formation of metal particles that were shown by transmission electron diffraction to be oriented with respect to the

ZrO_2 lattice [5,6]. The support effects observed with ZrO_2 are not complicated by the formation of overlayers that partially cover the metal particle, since ZrO_2, in contrast to reducible oxides such as TiO_2 and Nb_2O_5 [1,2], is a difficult-to-reduce support. Nonetheless, the cause of the support effects observed with ZrO_2 is not yet well understood; electronic effects [9] or direct interaction of reactants with the ZrO_2 support have been suggested [10].

One approach to understanding the metal–support interface, articulated decades ago by Schwab (and recently summarized [11]), involves the investigation of metal oxides supported on metals. Such samples offer experimental advantages; for example the high electrical conductivity of the support allows characterization by electron spectroscopies and scanning tunneling microscopy (STM). Two-dimensional films of ZrO_2 on Pt(111) have been observed previously; oxidation gave bulk ZrO_2 with the fcc structure [12,13]. ZrO_2 supported on Pd black has been characterized by extended X-ray absorption fine structure (EXAFS) spectra which showed that tetragonal ZrO_2 was formed after reduction at 500°C, whereas a previously unknown ZrO_2 crystal structure was formed after oxidation at 400°C; this structure was suggested to be stabilized by Pd oxide at the metal–metal oxide interface [14].

The goals of the research reported here were to extend the EXAFS investigation and to characterize ZrO_2 supported on Pd(100) by STM combined with TS to understand better the local geometric and electronic structure.

2. Experimental methods

2.1. MATERIALS

A Pd(100) single crystal was prepared from a Pd rod by standard methods and polished with diamond powder (0.25 μm) followed by corundum powder (0.05 μm). All the experiments were done with one crystal. $[Zr(OC_2H_5)_4]$ (Soekawa, 99.95%) was used without further purification. H_2 and He (Matheson, 99.999%) were purified by passage through traps containing activated copper oxide and molecular sieve zeolite particles to remove traces of O_2 and water, respectively.

2.2. SAMPLE PREPARATION

The Pd-supported sample was prepared by vapor deposition of $[Zr(OC_2H_5)_4]$. $[Zr(OC_2H_5)_4]$ powder was heated to about 150°C under vacuum ($\approx 10^{-3}$ Torr) and held for 3 h; the vapor was transported to a connecting flask on a vacuum line that held the Pd crystal at room temperature. Deposition of $[Zr(OC_2H_5)_4]$ on the walls of the flask was evident. The single crystal of Pd with the deposited $[Zr(OC_2H_5)_4]$ was oxidized by treatment in a quartz tube that was open to air; the sample was heated at a rate of approximately 12.5°C/min to 400°C and held

for 1 min. The sample was cooled in air to room temperature. The sample was subsequently reduced by treatment in H_2 in the quartz tube; it was heated at a rate of 8°C/min to 500°C and held for 1 h. It was then cooled to room temperature in flowing He and transferred under He to a Braun glovebox in which the O_2 and H_2O concentrations were < 0.2 and < 2 ppm, respectively. Auger electron spectroscopy did not detect significant contamination by carbon or sulfur of the samples prepared in this fashion; no XPS experiments were performed.

2.3. STM EXPERIMENTS

The experiments were carried out with the untreated Pd single crystal and with the sample prepared from $[Zr(OC_2H_5)_4]$ in the oxidized and reduced forms. The experiments were performed in air with an LK Technologies (Bloomington, IN) model 1000 scanning tunneling microscope. Mechanically formed Pt tips were used. Post image processing of the images involved low pass filtering to remove high-frequency noise and histogram equalization to enhance contrast. Scanning was in the constant-current mode with a positive sample bias of 100 mV and a tunneling current of 1.0 nA. Tunneling spectra were recorded by first stabilizing the tip position at the current and bias noted above for imaging and then disabling the servo-control that maintains constant tunneling current. The sample bias was ramped from -2 to $+2$ V with respect to the tip, and the tunneling current was monitored. The voltage axis in all the tunneling spectra represents the potential applied to the sample relative to that of the tip.

3. Results

3.1. Pd SINGLE CRYSTAL

An STM image of Pd(100) (fig. 1a) represents the sample prior to chemical pretreatment. The surface was quite smooth and featureless. A typical I–V spectrum (fig. 1b) taken atop the Pd surface shows the absence of a band gap (plateau behavior around the origin) [15]. Metals, of course, do not exhibit a band gap. Thus, this spectrum served as a fingerprint of the exposed metallic regions of the surface after chemical pretreatment.

3.2. OXIDIZED SAMPLE PREPARED FROM $[Zr(OC_2H_5)_4]$ ON Pd(100)

A typical STM image of the Pd(100) surface after chemical pretreatment under oxidative conditions is shown in fig. 2a along with the line profile (fig. 2b) measured between points labeled A and B on the image. The deposited overlayers ("bright" regions of the image) are smooth and featureless and are of

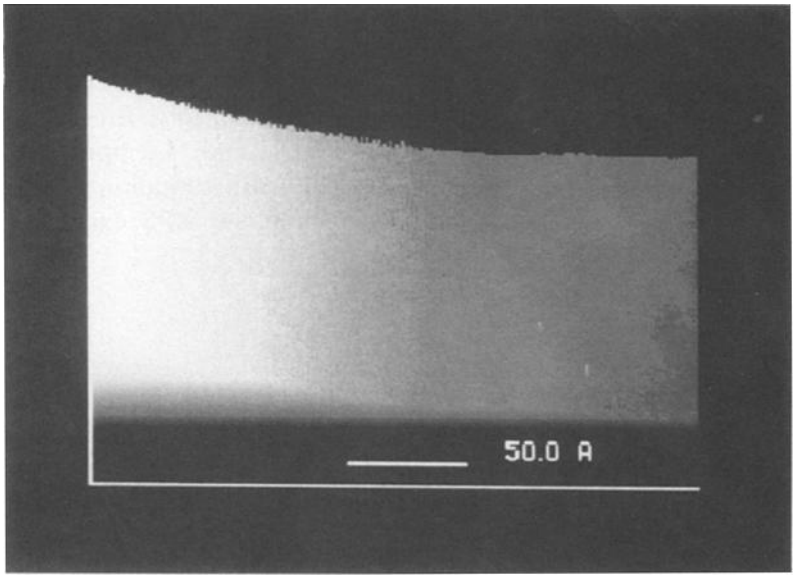

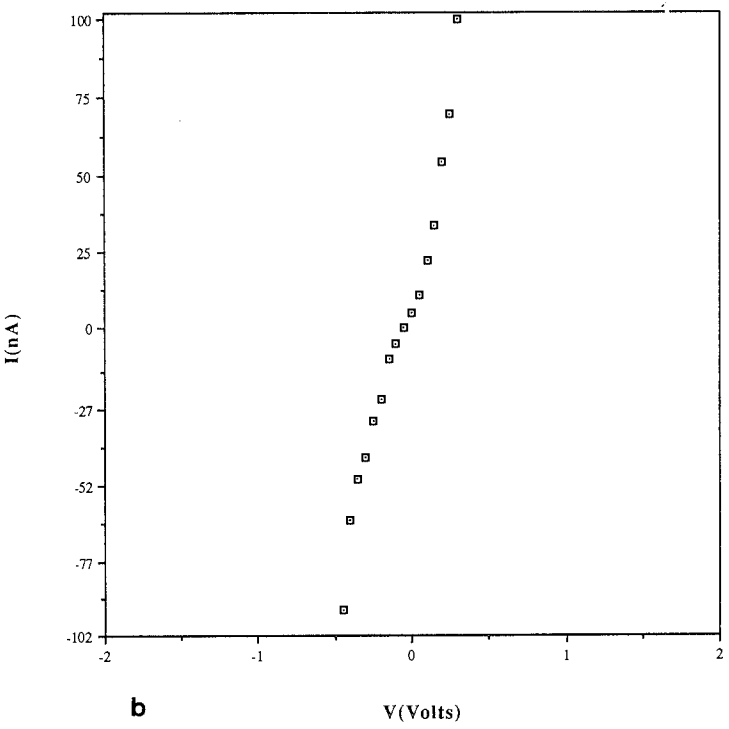

Fig. 1. (a) STM image of Pd(100) prior to chemical pretreatment; z-range = 82.7 Å. (b) $I-V$ spectrum of Pd(100) prior to chemical pretreatment. Spectrum is consistent with that of a metallic surface.

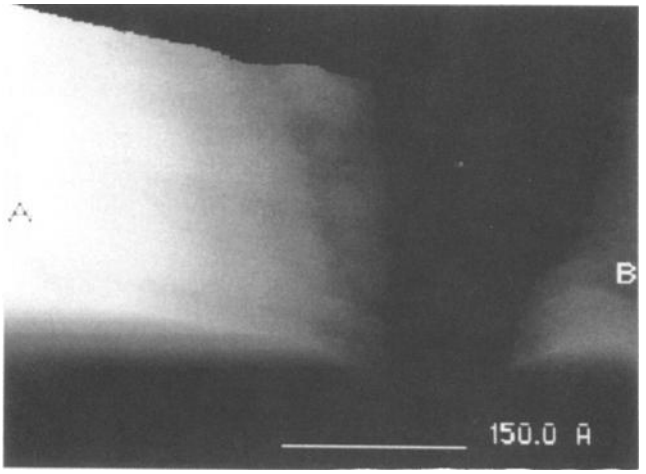

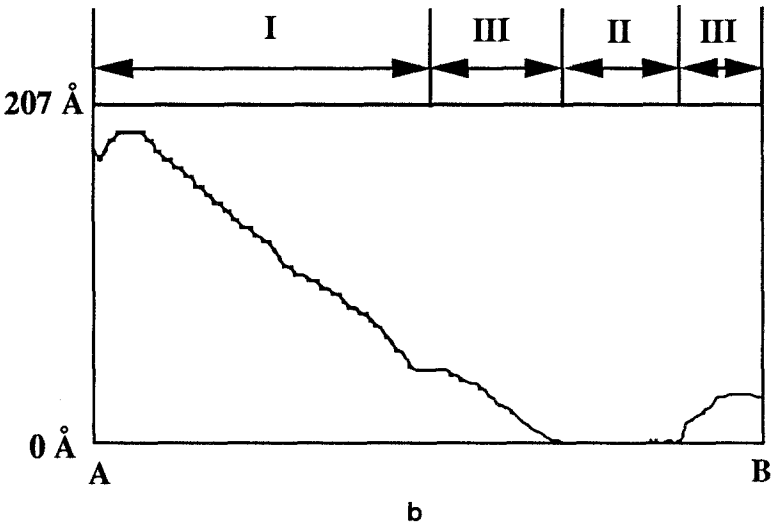

Fig. 2. STM image (a) and line profile (b) of ZrO_2/Pd(100) after oxidative pretreatment. Bright regions of the images are taken to be ZrO_2 and the dark region is the Pd(100) support. Regions I, II, and III denoted in the line profile indicate three electronically distinct regions of the surface: (I) semiconducting ZrO_2 overlayer, (II) boundary between overlayer and substrate, and (III) metallic Pd(100) substrate; z-range = 207 Å.

varying thickness, up to 150 Å above the Pd(100) substrate ("dark" regions of the image). It should be noted, however, that measurements along the z-direction must be regarded as more qualitative in nature for surfaces with non-constant work function than for compositionally uniform surfaces. Examination of

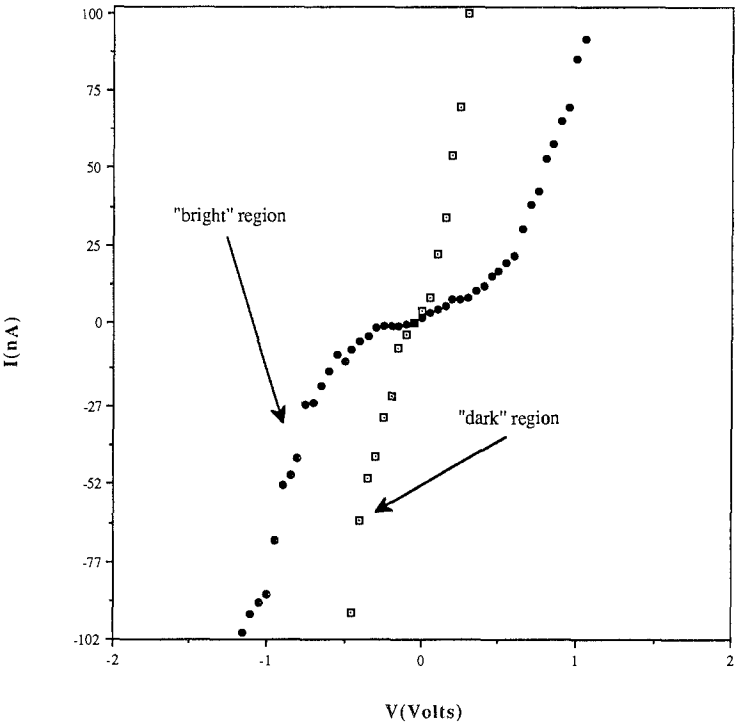

Fig. 3. Typical $I-V$ spectra taken atop "bright" and "dark" regions of the images shown in figs. 2a and 5a. Bright regions are semiconducting and dark regions are metallic.

larger scan areas revealed that the overlayer covered much of the surface. No discrete "particles" or islands were seen.

$I-V$ spectra taken atop the overlayer and Pd substrate (regions I and II of the line profiles, respectively) shown in fig. 3 indicate that the two areas are chemically and electronically inequivalent. The $I-V$ spectrum of the "dark" region (region II in the line profile) is consistent with that of bare Pd(100), whereas the spectrum of the bright region (region I in the line profile) is consistent with that of a non-rectifying semiconductor surface having a band gap of ≈ 0.8 eV. (The band gap is taken as the width of the plateau in the $I-V$ spectrum lying between -0.5 and $+0.3$ V in fig. 3.)

An $I-V$ spectrum taken atop the boundary between the ZrO_2 and the exposed Pd (region III of the line profile) is shown in fig. 4. The spectrum shows a negative differential resistance (NDR) peak at an applied bias of -0.45 V. Thus, this boundary is clearly electronically distinct from the ZrO_2 phase and from the Pd support.

3.3. REDUCED SAMPLE PREPARED FROM $[Zr(OC_2H_5)_4]$ ON Pd(100)

A typical STM image of the ZrO_2/Pd(100) sample after reductive pretreatment is shown in fig. 5a along with a line profile (fig. 5b) measured between

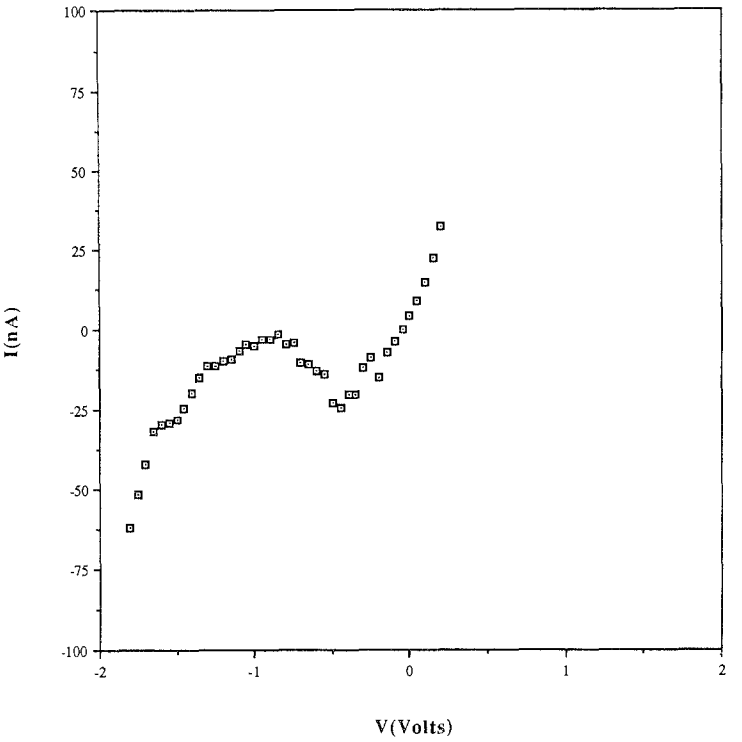

Fig. 4. I–V spectrum taken atop interfacial region between ZrO_2 and Pd(100) on the oxidized sample (i.e. region II of the line profile in fig. 2b). This spectrum exhibits negative differential resistance.

points A and B labeled in the image. Topographically, the image of the reduced sample is quite different from that of the oxidized sample. A much more distinct boundary exists between the overlayer and the substrate in the reduced sample. The ZrO_2 overlayer in the reduced sample is more "particle-like" than that in the oxidized sample, in which the overlayers appear to form a nearly continuous coating of non-uniform thickness. The ZrO_2 layer was also seen to be rougher in the reduced sample.

As for the oxidized sample, I–V spectra showed that the bright and dark regions of the images were semiconducting and metallic, respectively (fig. 1b). However, no region of the surface exhibited the negative differential resistance behavior that was observed for the oxidized sample (fig. 4). The surface morphology of the reduced sample was also different from that of the oxidized sample. The I–V data, therefore, indicate the presence of only two electronically distinct regions (metallic and semiconducting) on the surface.

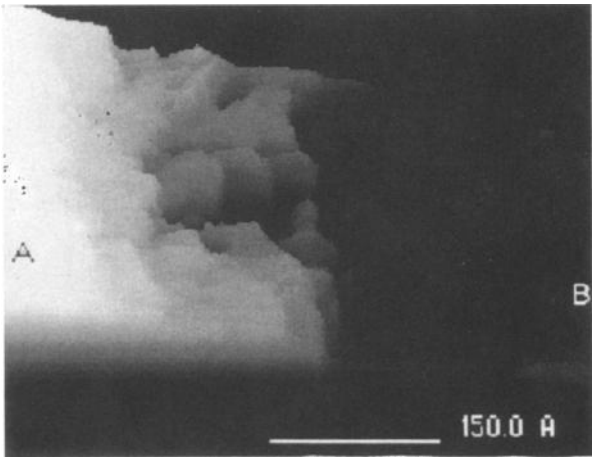

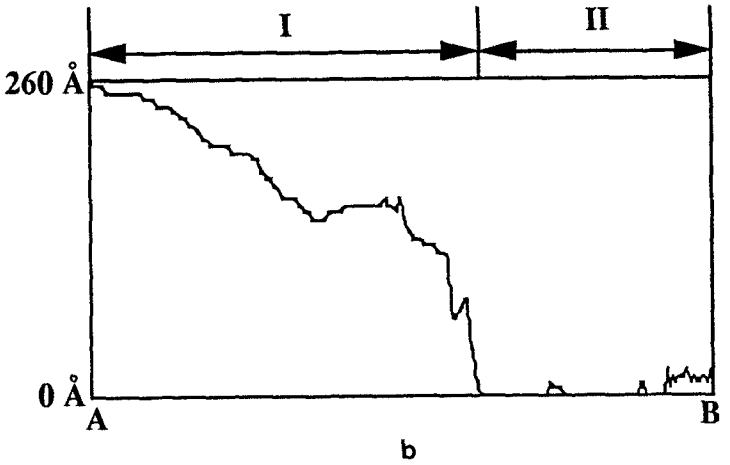

Fig. 5. STM image (a) and line profile (b) of ZrO_2 /Pd(100) after reductive pretreatment. Bright and dark portions of the image and regions of the line profile are assigned as in fig. 2b. Region III was not seen in the reduced sample; z-range = 260 Å.

4. Discussion

Samples similar to the ones investigated in this work have been prepared on Pd powder supports and characterized by X-ray absorption spectroscopy [14]. The X-ray absorption near edge structure data indicate that the Zr in the samples prepared analogously to those of this work was in the +4 oxidation state. Thus we infer that the Zr species in the oxidized and reduced samples were semiconducting oxides. The I–V data support this inference.

The STM data identify distinct phases on the sample surface, with the zirconium oxides being present in discrete phases that are dispersed on the Pd surface. Thus the STM results show that the preparation was successful in giving a model dispersed metal oxide on a metal support. I–V spectra indicate three distinct regions of the surface of the oxidized sample. The "bright" and "dark" regions in the images are taken to represent the semiconducting ZrO_2 and the metallic Pd(100) support, respectively. The third region of the surface, the interface between the ZrO_2 and Pd(100), showed NDR behavior in the I–V spectra. Physical phenomena that can give rise to NDR in TS experiments have been discussed previously [16–18]. The presence of local regions on the surface which exhibit NDR requires localized electronic states distinct from those characteristic of the other large-scale features of the surface. These electronically distinct interface regions may be regions of monolayer metal oxide formation on the Pd(100) surface. We have previously observed localized NDR behavior, for example, for discrete metal oxide structures on conducting substrates [19]. Such a monolayer might be palladium oxide, which Asakura and Iwasawa [14] inferred (on the basis of EXAFS data) to be a possible species on the oxidized sample.

These EXAFS data indicate that in the oxidized form of a sample prepared from Pd black (powder) and $[Zr(OC_2H_5)_4]$, the zirconium oxide was present in very thin layers that were inferred to be in registry with the Pd support. The EXAFS data led to the inference that the structure of the Zr oxide was different from the known structures of bulk zirconium oxides. However, treatment of the sample in H_2 led to a restructuring of the zirconium oxide. The EXAFS data then indicated the presence of zirconium oxide with Zr in tetragonal surroundings, consistent with the presence of a known bulk phase. The changes were found by EXAFS spectroscopy to be reversible. These results imply that the metal–metal oxide interface changed significantly upon reduction and oxidation of the sample.

The STM data are consistent with these conclusions, showing that the interface between the metal oxide and metal changed as a result of the treatment in H_2. Evidence for the change in the interface structure is provided by (1) STM images indicating the increased sharpness of the edges separating the metal and metal oxide phases on the surface and (2) the I–V curves, which indicate that a third phase is present in the region between the metal and metal oxide phases in the oxidized sample but not in the reduced sample.

These STM data suggest that the zirconium oxide in the oxidized sample wets the Pd surface, whereas the zirconium oxide in the reduced sample does not. The EXAFS results are consistent with this interpretation. We infer that the zirconium oxide in the oxidized sample was spread into a thin layer, with the oxide structure perhaps determined by the structure of the underlying support. In contrast, the structure of the reduced zirconium oxide on Pd is a bulk structure, influenced only little by the support.

There is extensive evidence that oxides of reducible metals such as Ti and Nb, when used as supports for metal crystallites, can, after high-temperature reduction, form structures that creep onto the dispersed metals and may nearly cover them [1,2]. ZrO_2 does not behave like these reducible metal oxide supports; it has not been observed to creep onto metals dispersed on it. The EXAFS results mentioned above are consistent with the slight reducibility of the zirconium oxide. ESR spectra indicate that ZrO_2 is reduced to Zr^{3+} only after reduction in H_2 at 873 K [20].

Thus it is inferred that the effect of ZrO_2 as a support is not associated with its migration onto the metal. The present results do, however, show a change in the structure of the metal–metal oxide interface upon reduction of the sample. These results, combined with the above-mentioned EXAFS results, are consistent with the occurrence of unique structures at metal–zirconium oxide interfaces.

Acknowledgement

This research was supported by the US Department of Energy, Office of Energy Research, Office of Basic Energy Sciences (Contracts FG02-87ER13790 and FG02-84ER13290). The international collaboration was supported by the Japan Society for the Promotion of Science (USA–Japan Cooperative Research Program) and the National Science Foundation (Grant INT-9016911).

References

[1] S.A. Stevenson, J.A. Dumesic, R.T.K. Baker and E. Ruckenstein, eds., *Metal–Support Interactions in Catalysis, Sintering, and Redispersion* (Van Nostrand Reinhold, New York, 1987).
[2] G.L. Haller and D.E. Resasco, Adv. Catal. 36 (1989) 36.
[3] D.C. Koningsberger and B.C. Gates, Catal. Lett. 14 (1992) 271.
[4] C. Schild, A. Wokaun and A. Baiker, J. Mol. Catal. 69 (1991) 347.
[5] G.S. Zafiris and R.J. Gorte, J. Catal. 132 (1991) 275.
[6] S. Roberts and R.J. Gorte, J. Phys. Chem. 95 (1991) 5600.
[7] M. Ichikawa, K. Sekizawa, K. Shikakura and M. Kawai, J. Mol. Catal. 11 (1981) 167.
[8] C. Mazzocchia, E. Tempesti, P. Gronchi, L. Giuffrè and L. Zanderighi, J. Catal. 111 (1988) 345.
[9] H. Yoshitake and Y. Iwasawa, to be published.
[10] E. Guglielminotti, J. Catal. 120 (1989) 287.
[11] M. Boudart and G. Djéga-Mariadassou, *Kinetics of Heterogeneous Catalytic Reactions* (Princeton Univ. Press, Princeton, NJ, 1984) p. 207.
[12] V. Maurice, M. Salmeron and G.A. Somorjai, Surf. Sci. 237 (1990) 116.
[13] V. Maurice, K. Takeuchi, M. Salmeron and G.A. Somorjai, Surf. Sci. 250 (1991) 99.
[14] K. Asakura and Y. Iwasawa, J. Phys. Chem., to be published.

[15] L.J. Whitman, J.A. Stroscio, R.A. Dragoset and R.J. Celotta, Phys. Rev. Lett. 66 (1991) 1338.
[16] M.G. Youngquist and J.D. Baldeschwieler, J. Vac. Sci. Technol. B9 (1991) 1083.
[17] I.-W. Lyo and P. Avouris, Science 245 (1989) 1369.
[18] P. Bedrossian, D.M. Chen, K. Mortensen, and J.A. Golovchenko, Nature 342 (1989) 258.
[19] B.A. Watson, M.A. Barteau, L. Haggerty, A.M. Lenhoff and R.S. Weber, Langmuir 8 (1992) 1145.
[20] A. Gervasini, F. Morazzoni, D. Strumolo, F. Pinna, G. Strukul and L. Zanderighi, J. Chem. Soc. Faraday Trans. I 82 (1986) 1795.